Up-regulation of the inward rectifier K^+ current (I_{K1}) in the mouse heart accelerates and stabilizes rotors

Sami F. Noujaim[1]*, Sandeep V. Pandit[1]*, Omer Berenfeld[1], Karen Vikstrom[1], Marina Cerrone[1], Sergey Mironov[1], Michelle Zugermayr[1], Anatoli N. Lopatin[2] and José Jalife[1]

[1]*Institute for Cardiovascular Research and Department of Pharmacology, SUNY Upstate Medical University, Syracuse, NY, USA*
[2]*Department of Molecular and Integrative Physiology, University of Michigan, Ann Arbor, MI, USA*

Previous studies have suggested an important role for the inward rectifier K^+ current (I_{K1}) in stabilizing rotors responsible for ventricular tachycardia (VT) and fibrillation (VF). To test this hypothesis, we used a line of transgenic mice (TG) overexpressing Kir 2.1–green fluorescent protein (GFP) fusion protein in a cardiac-specific manner. Optical mapping of the epicardial surface in ventricles showed that the Langendorff-perfused TG hearts were able to sustain stable VT/VF for 350 ± 1181 s at a very high dominant frequency (DF) of 44.6 ± 4.3 Hz. In contrast, tachyarrhythmias in wild-type hearts (WT) were short-lived (3 ± 9 s), and the DF was 26.3 ± 5.2 Hz. The stable, high frequency, reentrant activity in TG hearts slowed down, and eventually terminated in the presence of 10 μM Ba^{2+}, suggesting an important role for I_{K1}. Moreover, by increasing I_{K1} density in a two-dimensional computer model having realistic mouse ionic and action potential properties, a highly stable, fast rotor (≈45 Hz) could be induced. Simulations suggested that the TG hearts allowed such a fast and stable rotor because of both greater outward conductance at the core and shortened action potential duration in the core vicinity, as well as increased excitability, in part due to faster recovery of Na^+ current. The latter resulted in a larger rate of increase in the local conduction velocity as a function of the distance from the core in TG compared to WT hearts, in both simulations and experiments. Finally, simulations showed that rotor frequencies were more sensitive to changes (doubling) in I_{K1}, compared to other K^+ currents. In combination, these results provide the first direct evidence that I_{K1} up-regulation in the mouse heart is a substrate for stable and very fast rotors.

(Resubmitted 20 September 2006; accepted after revision 3 November 2006; first published online 9 November 2006)
Corresponding author J. Jalife: Department of Pharmacology, SUNY Upstate Medical University, 750 E. Adams St, Syracuse, NY 13210, USA. Email: jalifej@upstate.edu

The role of the inward rectifier K^+ current (I_{K1}) in arrhythmogenesis has been the focus of experimental studies in the guinea-pig heart (Samie *et al*. 2001; Warren *et al*. 2003) and of computer simulations (Beaumont *et al*. 1998; Fox *et al*. 2002; Zhang *et al*. 2005).

In cardiac myocytes, I_{K1} sets the resting membrane potential, controls the approach to threshold upon depolarization, and modulates the terminal phase of repolarization (Lopatin & Nichols, 2001; Miake *et al*. 2003). The importance of I_{K1} in determining rotor dynamics was first suggested in computer simulations (Beaumont *et al*. 1998), which led us to analyse its role in the mechanism of ventricular fibrillation (VF) (Samie *et al*. 2001; Warren *et al*. 2003). In the guinea-pig heart, Kir2.1 and Kir2.3 proteins (Kir2.x is the molecular correlate of I_{K1}) are more abundant in the left ventricle (LV) than in the right ventricle (RV) (Warren *et al*. 2003), with correspondingly greater outward currents in the myocytes of the LV compared to the RV. This results in a shorter action potential duration (APD), allowing rotors to stabilize in the LV. On the other hand, less outward current in the RV seems to create a favourable substrate for the wavefront to interact with its tail, which in the guinea-pig model prevents the RV from maintaining stable spiral waves (Samie *et al*. 2001). Pharmacological reduction of I_{K1} density using $BaCl_2$ at low concentrations has been shown to terminate stable VF, which supports a role of this current in rotor dynamics (Warren *et al*. 2003). However, to date, direct proof for the role of inward rectifier channels in the control of rotor stability and frequency is lacking.

Genetically engineered mice represent invaluable tools in which the electrophysiological consequences of manipulating ion channels at the molecular level can be

*S. F. Noujaim and S. V. Pandit contributed equally to this work.

 DOI: 10.1113/jphysiol.2006.121475

directly determined. Recently, Li *et al*. (2004) generated a transgenic mouse in which I_{K1} was up-regulated by overexpressing the Kir2.1 (green fluorescent protein (GFP)-tagged) protein in the heart under control of the α-myosin heavy chain promoter. Two viable lines (line 1 and 2) that overexpressed the Kir2.1–GFP fusion protein were generated. Surface ECG recordings from anaesthetized line 2 mice revealed dramatic abnormalities of excitability including short corrected QT interval (QTc), slowed heart rate, junctional escape, atrioventricular block, atrial flutter and sudden death. Line 1 mice survived longer than line 2 mice, and had a prolonged QRS interval and shortened QTc interval compared to WT mice. The effective refractory period in isolated hearts was reduced in both lines (Li *et al*. 2004). Here we present original data from optical mapping experiments in line 1 mice and parallel computer simulations that demonstrate that I_{K1} has a crucial role in controlling frequency and stability of rotors responsible for VT/VF in the mouse heart.

Methods

Animals

Experiments were carried out in adult wild-type (WT; $n = 12$) and transgenic mice (TG; $n = 21$). For heart isolation, animals were heparinized (0.5 U g^{-1} I.P.) and then anaesthetized with a ketamine (116 mg kg^{-1})–acepromazine (11 mg kg^{-1}) mixture injected I.P. Hearts were rapidly excised through a midline thoracotomy, after which the animals die, with minimal pain and discomfort. All animal handling protocols conformed to institutional and NIH guidelines (The SUNY Upstate Medical University Committee on Humane Use of Animals, and the 2000 Report of the American Veterinary Medical Association Panel on Euthanasia).

Hypertrophy assessment

Hearts were collected from age- and gender-matched animals. After rinsing with Tyrode solution, the RV was dissected free from the LV and septum under a stereomicroscope. The weights of the animal, heart, LV and RV were recorded. Tissues were then flash-frozen in liquid nitrogen and stored at -70°C. Total RNA was isolated (Chomczynski & Sacchi, 1987) and then 3 μg LV RNA was immobilized on nylon membrane using a slot blot apparatus. Random-primed ^{32}P-labelled probes were generated using a PstI fragment from a rat atrial natriuretic factor (ANF) cDNA (Seidman *et al*. 1984) or a PstI fragment from a rat glyceraldehyde-3-phosphate-dehydrogenase (GAPDH) cDNA (Piechaczyk *et al*. 1984) as templates. Oligonucleotide probes recognizing murine β-myosin heavy chain (β-Myh) (5′-TGTTGCAAAGGCTCCAGGTCTGAGGGCTTC-3′) or murine α-skeletal actin (5′-CTGCTGCTCTGACTCTGGCCCTGGGTGCCGAGGGTAGG-3′) were end-labelled using T4 Polynucleotide Kinase. We used yeast tRNA (ytRNA) as negative control, and as positive controls, we used neonatal mouse hearts and skeletal muscle. Membranes were hybridized using UltraHybe (Ambion, Austin, TX, USA). Following washing, the membrane was exposed to storage-phosphor plates and images were acquired using a Molecular Dynamics PhosphoImager (Sunnyvale, CA, USA). The intensity of the signals was quantified using the Quantity One program and expression levels were normalized to GAPDH (Bio-Rad).

Isolation, perfusion and optical mapping of mouse hearts

The heart was excised through thoracotomy and subsequently connected to a Langendorff-perfusion system to be continuously perfused with warm oxygenated Tyrode solution with bicarbonate as buffer. The pH was brought to 7.4 with NaOH and the solution was continuously bubbled with 95% O_2–5% CO_2. The temperature of the perfusate was maintained at $36 \pm 1^{\circ}$C as described previously (Tamaddon *et al*. 2000). The heart was placed in the well of a custom-made plastic chamber maintained at 35–36°C and allowed to equilibrate for 10 min. Optical mapping was performed, using a high-resolution 64 pixel × 64 pixel CCD camera (DALSA) recording at a rate of 400–600 frames s^{-1}, and a spatial resolution of 109 μm. The voltage sensitive dye used was Di-4-ANEPPS (Vaidya *et al*. 1999; Tamaddon *et al*. 2000; Bagwe *et al*. 2005). Hearts were unrestrained and no electromechanical uncouplers were used. The dimensions of our field of view were 7 mm × 7 mm.

Volume-conducted ECG recordings and pacing protocol

Volume-conducted ECGs were recorded at 1 kHz in isolated hearts as described previously (Samie *et al*. 2001). Power spectra of reentry episodes were created by Fast Fourier Transform (FFT) analysis using Origin 7.0 software. To induce arrhythmias, burst pacing was used where a unipolar suction electrode positioned on the RV outflow area delivered short bursts of 5 ms in duration and at cycle lengths between 15 and 30 ms at two times diastolic threshold.

Phase movies and dominant frequency maps

Phase movies for the supplemental video clips were constructed, as has been described previously (Samie *et al*. 2001). As explained in detail previously (Berenfeld *et al*. 2002), to generate the dominant frequency (DF) maps,

FFT was performed on the optical signal from each pixel of the epicardial optical signals. The DF was determined for each pixel and maps of spatial DF distribution were constructed.

Activation maps and conduction velocity measurements during reentry

Activation maps for reentry were generated by calculating, for each pixel, the activation time during one rotation. For the computation of conduction velocity (CV) maps, the magnitude of local conduction vectors was determined on the basis of the activation times of surrounding pixels during one rotation, as described (Morley *et al*. 1999). Subsequently, to generate the CV *versus* distance plots, the magnitudes of the conduction vectors around the core at increasing distance, were averaged and plotted against the distance as mean CV ± s.d. The weighted best-fit line was generated using Origin 7.0 software. Weighting was applied as the s.d. of the CV. The 95% upper and lower confidence limits were also calculated. Slopes are reported as the weighted slope ±95% confidence limit. If the lower 95% confidence limit of a slope did not reach 0, then the slope was different from 0. Two slopes were not considered different if the ranges of their 95% confidence limits overlapped. Core diameter during two successive rotations was measured using the time–space plot (TSP) in three WT and three TG rotors as well as in simulated WT and TG reentry. For details of TSP analysis, see Supplemental material.

Statistical analyses

The data are presented as means ± standard deviation of the mean (s.d.). Analysis of variance (ANOVA) was applied as appropriate. Student's *t* test (unpaired) was used when needed. The level of statistical significance was taken at $P < 0.05$.

Computer simulations

Mathematical models of rodent (rat and mouse) ventricular action potentials (APs) have been published recently (Pandit *et al*. 2001; Bondarenko *et al*. 2004). However, both models simulate the cardiac AP at room temperature (22°C), and include descriptors for ionic currents and intracellular ion fluxes, which are either Hodgkin-Huxley-type differential equations, or more complex Markovian formulations. Markovian models and detailed subcellular Ca^{2+} formulations describe physiological behaviour more realistically, but at an enhanced computational cost. Therefore, for the purposes of this study, we have developed a simplified (all intracellular ion concentrations, including Ca^{2+}, are constant), yet ionically realistic mathematical model of the mouse ventricular AP at physiological temperatures (37°C). This single-cell model was then incorporated into a two-dimensional (2D) sheet of mouse ventricular cells to study reentry as in a recent study (Pandit *et al*. 2005). The main goal was to investigate the effects of up-regulation in I_{K1} density on rotor dynamics. A detailed discussion on the development and validation of this model is presented in the Supplemental material, which also includes a description of the 2D model, and the computational methods used therein.

Results

Arrhythmogenesis in WT and TG hearts

As illustrated in Fig. 1, sustained reentry was inducible by ventricular burst pacing (cycle length (CL), 15–30 ms) in TG but not in WT hearts. In Fig. 1*A*, the top trace shows

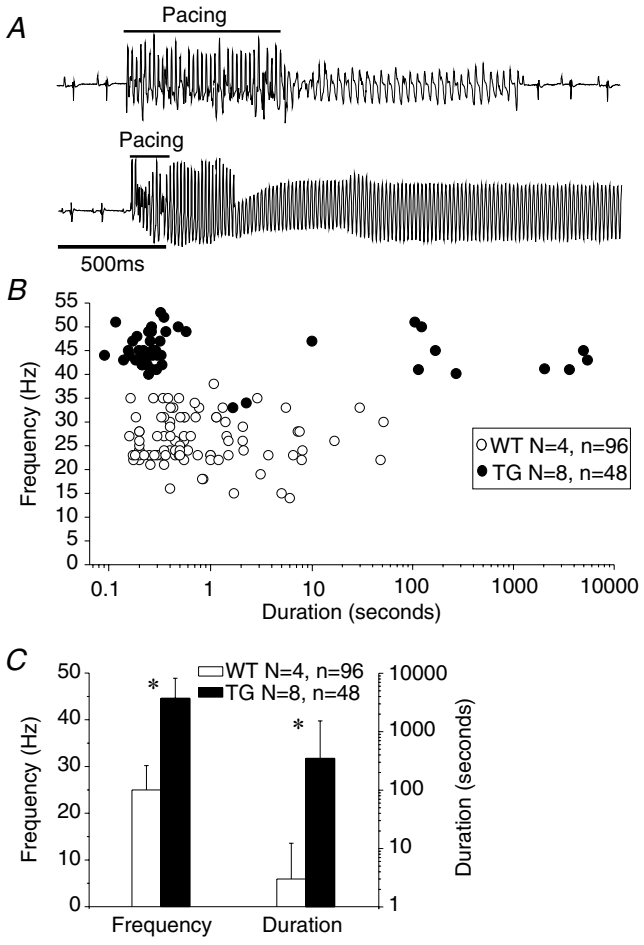

Figure 1. Burst pacing-induced VT/VF
A, volume-conducted ECGs of representative WT (top) and TG (bottom) hearts. *B*, composite plot of the duration and frequency of tachyarrhythmia episodes in four WT and eight TG hearts. *C*, average duration and frequency of arrhythmias in four WT and eight TG hearts. *$P < 0.001$.

a short episode of non-sustained VF in a WT heart, which reverted back to sinus rhythm. As shown by the lower trace, in a TG heart, burst pacing caused a fast monomorphic ventricular tachycardia (VT) that was sustained. Composite data presented in Fig. 1*B* highlight differences between the two groups. In eight TG hearts, 48 episodes of VT or VF had an average frequency of 44.6 ± 4.3 Hz and an average duration of 350 ± 1181 s. In four of these hearts, the arrhythmia lasted more than 30 min, and in one heart, it was not possible to induce an arrhythmic episode lasting more than 10 s. Instead, episodes of high frequency, but short duration were elicited. On the other hand, the average duration of 96 episodes in four WT hearts was 3 ± 9 s and the frequency was 26.2 ± 5.2 Hz. None of the WT hearts was able to accommodate a sustained arrhythmia for more than 60 s. Fig. 1*C* shows a plot of the average duration and frequency of the tachyarrhythmic episodes in the WT and TG hearts. There was statistical difference between duration (WT, 3 ± 9; TG, 350 ± 1181 s, $P < 0.001$) and frequency (WT, 26.2 ± 5.2; TG, 44.6 ± 4.3 Hz, $P < 0.001$) of arrhythmias in the two groups.

Dynamics of fibrillation

Figure 2 shows volume-conducted ECGs, DF maps and power spectral plots from representative WT and TG hearts in VF. In both cases the ECGs (top) are compound, with polymorphic wave shapes characteristic of VF, but the complexes are narrower in the TG compared to the WT heart. In both cases the arrhythmias were complex. In the WT heart, the DF map (middle left) reveals a 33 Hz frequency domain (yellow) in addition to other slower domains, consistent with the power spectrum of the ECG trace (bottom left), which displays a DF of 34 Hz along with additional small peaks in an overall pattern that is typical of VF (Samie *et al*. 2000). The DF map of the TG heart (middle right) shows a domain (white) of 56 Hz, coexisting with other slower frequency domains. The power spectrum of the ECG (bottom right) displays a large peak at 56 Hz coexisting with multiple other smaller peaks. Again, this pattern is indistinguishable from VF.

I_{K1} blockade terminates reentry

To test whether the high frequencies of sustained reentry in the TG hearts were attributable to an enhanced inward rectifier current density, we perfused the heart with 10 μM $BaCl_2$, which selectively blocks I_{K1} at concentrations in the micromolar range (DiFrancesco *et al*. 1984; Kubo *et al*. 1993; Warren *et al*. 2003). In Fig. 3*A*, the left column shows the ECG, DF map and power spectrum at the onset of arrhythmia in a representative experiment. Burst pacing resulted in sustained reentry at 46 Hz. The middle column shows the same heart after 1 min; the DF remained at 48 Hz. Upon perfusion with 10 μM Ba^{2+}, reentry slowed down to about 24 Hz and then stopped after ~1.5 min of exposure. In Fig. 3*B*, data from five such experiments are compiled. Frequency at each time point was normalized to the dominant frequency at the onset of

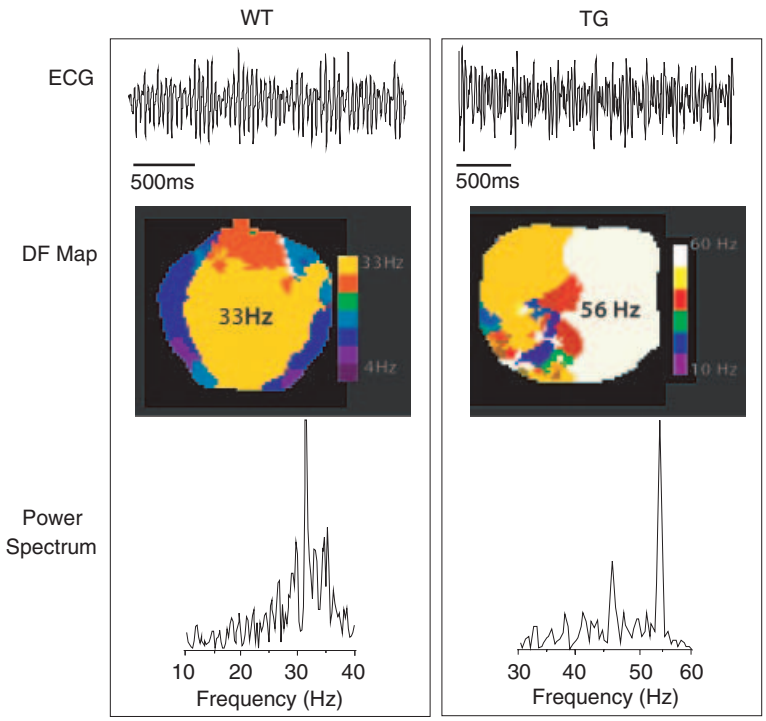

Figure 2. Ventricular fibrillation in WT (left) and TG (right) hearts
Top, ECGs; middle, dominant frequency (DF) maps; bottom, corresponding power spectra of the ECG traces. Colour scales: WT, 4–33 Hz; TG, 10–60 Hz. See Supplemental material for examples of 'WT VF' and 'TG VF' movies.

reentry. In all cases, perfusion with 10 μM Ba^{2+} reduced the DF by about 50% and then converted reentry to sinus rhythm after an average time of 5.5 ± 4 min. In one experiment, after 10 min washout, burst pacing recovered the reentrant activity with a frequency that was 73% of control (data not shown).

Does hypertrophy contribute to high rotor frequency?

Li *et al*. (2004) reported that the ventricles of line 1 mice, as used here, had a tendency to develop mild hypertrophy. Therefore, to rule out the possibility that hypertrophy or molecular remodelling somehow contributed to the electrophysiological changes, we compared wet weights of whole heart, LV and RV of six WT *versus* six TG hearts. As demonstrated in Fig. 4*A*, no evidence of hypertrophy was seen when tissue weights were normalized to body weight. The results were negative also for absolute wet weight values, and when the weights were normalized to tibial length (not shown). Moreover, to determine whether there was molecular remodelling in the absence of overt cardiac hypertrophy, left ventricular RNAs from three WT and three TG hearts were examined by slot blot analysis to assess alterations in the abundance of three markers for pathological remodelling: ANF, β-Myh and α skeletal actin. As shown in Fig. 4*B* and *C*, no statistically significant difference in the abundance of these markers was seen between WT and TG hearts. Altogether, these results rule out completely the possibility that hypertrophy contributed to the increased reentry frequency and sustainability demonstrated above for line 1 mice.

Mechanism of rotor acceleration and stabilization

We developed a new, simplified, single-cell ionic model of the mouse ventricular AP at physiological temperature

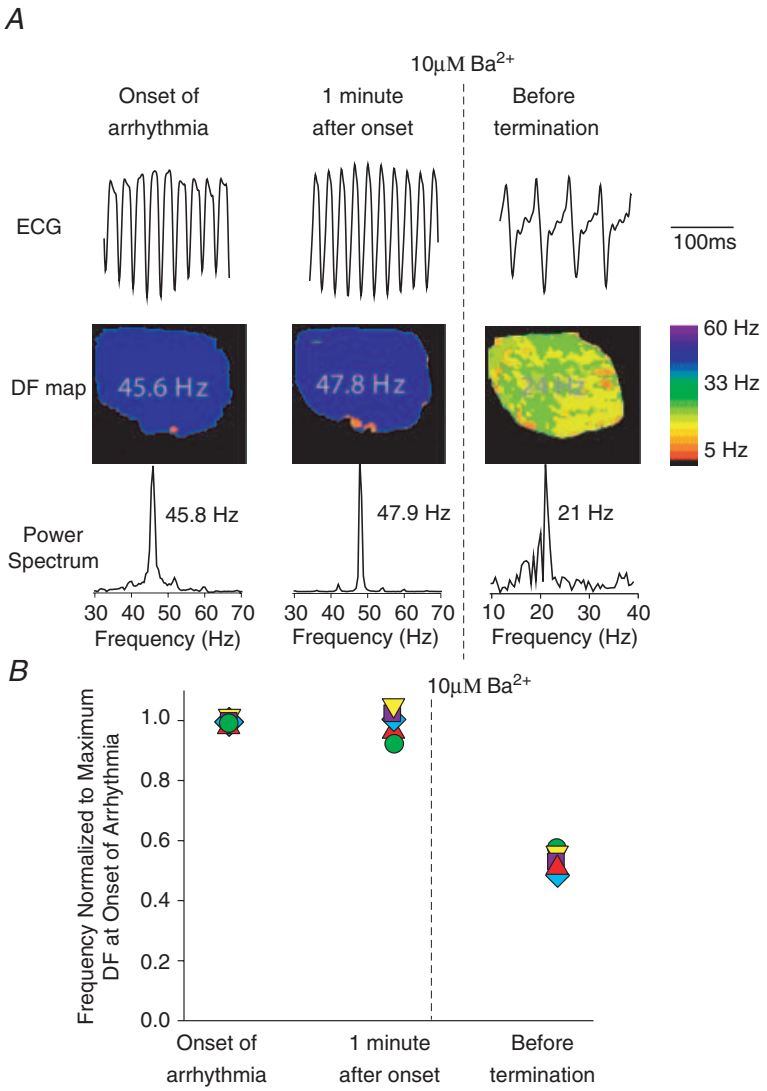

Figure 3. Effects of 10 μM Ba^{2+} on reentry frequency and stability in TG hearts
A, representative experiment. Left, onset of reentry. Dominant frequency (DF) is ~46 Hz. Middle, 1 min after onset of reentry; DF is stable at ~48 Hz. Right, 1.5 min after onset of 10 μM Ba^{2+} perfusion; DF slowed down to 24 Hz. Reentry stopped immediately thereafter. *B*, composite data from five TG heart experiments. Frequency of activation is normalized to the maximal frequency in the DF map. Perfusion with 10 μM Ba^{2+} reduced reentry frequency by ~50% of control before termination.

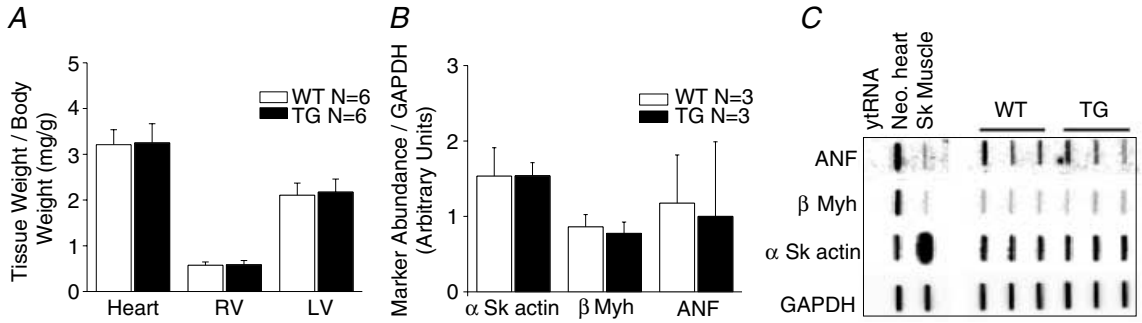

Figure 4. Assessment of hypertrophy
A, normalized weights of whole heart, and left (LV) and right ventricle (RV) in TG *versus* WT hearts. *B* and *C*, slot blot analysis of LV RNA from WT and TG hearts to show changes in message for atrial natriuretic factor (ANF), β-myosin heavy chain (β-Myh) and α skeletal actin. There are no statistical differences in any of the comparisons. ytRNA, yeast tRNA; Neo. Heart, neonatal mouse heart; Sk muscle, skeletal muscle.

(37°C), as detailed in the Supplemental material. The simulated mouse AP and the main currents underlying its plateau and repolarization phases are depicted in Fig. 5*A*. They include the transient outward K^+ current (I_{to}), the 4-aminopyridine-sensitive, slow delayed rectifier K^+ current (I_{Kslow}), the steady-state K^+ current (I_{ss}), the L-type Ca^{2+} current (I_{CaL}) and I_{K1}. Note that both I_{K1} and I_{ss} are almost an order magnitude smaller than other currents (for illustration purposes I_{K1} has been multiplied by a factor of 10). It can be seen that whereas I_{to}, I_{Kslow}, I_{ss} and I_{CaL} interact to produce the initial rapid repolarization, there is a late, slow repolarization phase where I_{K1} is the main repolarizing current (in this version of our model, the intracellular Ca^{2+} is fixed. Thus the Na^+–Ca^{2+} exchanger will not contribute substantially to the late repolarization; nevertheless the simulated AP mimics experimentally

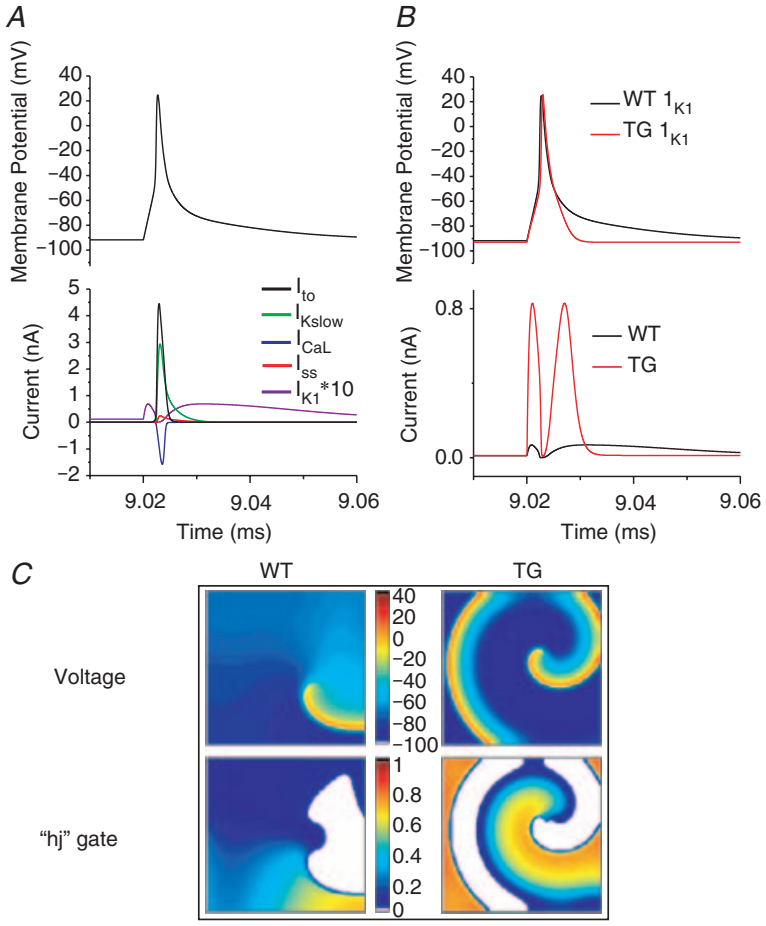

Figure 5. Simulated action potentials and reentry in WT and TG hearts
A, simulated mouse ventricular action potential and main currents involved in repolarization. I_{K1} is multiplied by a factor of 10 for illustration purposes. *B*, action potentials and respective underlying I_{K1} for WT (black) and TG (red) hearts. The conductance of I_{K1} in TG is 12 times greater than in the WT hearts. *C*, spatial distribution of transmembrane voltage (top) and inactivation gating variables ('hj' gates, bottom) of the I_{Na} during stable reentry in a 2 cm × 2 cm cardiac cell sheet. The diastolic potential is more hyperpolarized over a wider area in the TG heart sheet (~−94 mV), compared to the WT case (~−90 mV). The 'hj' gate map shows that the maximum availability of Na^+ channels in TG (0.808) exceeds that of the WT heart (0.684), and occupies a larger area during the excitable gap.

recorded ones in the presence of EGTA). A sharp increase in I_{K1} can be expected to induce a much faster terminal repolarization. This is shown in Fig. 5*B*, where the larger conductance of I_{K1} in the TG hearts (12 times that of the WT (Li *et al*. 2004)) causes a significant shortening of the AP, and a small hyperpolarization of the resting membrane potential, as would be expected. To simulate the AP in TG hearts, we also increased I_{ss} by 36% as seen experimentally (Li *et al*. 2004).

Next, the single-cell model was incorporated into an isotropic, uniform 2D sheet (2 cm × 2 cm), and cross-field stimulation was used to induce rotors, whose frequencies were ∼18.5 Hz and ∼45 Hz in WT and TG hearts, respectively. Figure 5*C* displays a representative snapshot of the distribution of membrane voltage, and the underlying inactivation gating variables ('hj') of the sodium current (I_{Na}) during simulated reentry in WT and TG hearts. The product of the 'h' and 'j' gates is representative of the excitability of the resting tissue, or the excitable gap. The voltage maps show that the wavelength is shorter and the diastolic potential is more hyperpolarized (darker blue) over a wider area in the TG cardiac sheet, compared to the WT (values of diastolic potentials were ∼−94 mV in TG *versus* ∼−90 mV in WT). This results in greater recovery of Na^+ channel availability (maximum value of 'hj' is 0.808 *versus* 0.684 in TG *versus* WT hearts). Furthermore, the accelerated final phase of repolarization results in a larger area in which Na^+ channels have recovered (orange), and thus greater excitability in front of the depolarization wavefront. These factors contribute in part to the higher rotor frequency seen in the TG hearts. Furthermore, as predicted by simulations presented in the Supplemental material, the lower excitability and larger wavelength in the WT hearts does not allow rotors to stabilize when the size of the tissue is reduced to 1 cm × 1 cm. In that case, the rotor terminates after about two rotations, which mimics experimental observations (see Fig. 1). In contrast, we could induce a sustained rotor at a frequency of ∼45 Hz in the TG hearts in a 1 cm × 1 cm sheet (data not shown).

I_{K1} up-regulation modifies local velocity during reentry

During sustained functional reentry, the local curvature of the wavefront increases towards the centre of rotation (core) and imposes a slowing of conduction velocity (CV) (Beaumont *et al*. 1998). This, together with an abbreviated APD in the immediate vicinity of the core (Beaumont *et al*. 1998) results in a sufficiently abbreviated wavelength to allow for stable rotation. Therefore, we sought to determine whether increased rotor frequency and stability induced by I_{K1} up-regulation in the TG heart is accompanied by a change in CV as a function of distance from the core. In Fig. 6 we present detailed analysis of rotor behaviour in simulated WT and TG rotors in a 2 cm × 2 cm sheet. To determine the effects of increasing I_{K1} on the local CV during reentry, we quantified the CV vectors in a circular area, with the core as its centre and a radius of 1.5 mm. The top panels are activation maps of the simulated WT and TG rotors. The cycle lengths of reentry were 54 and 22 ms for the respective WT and TG hearts. In the bottom panels, the average (± S.D.) local velocities at each step distance are

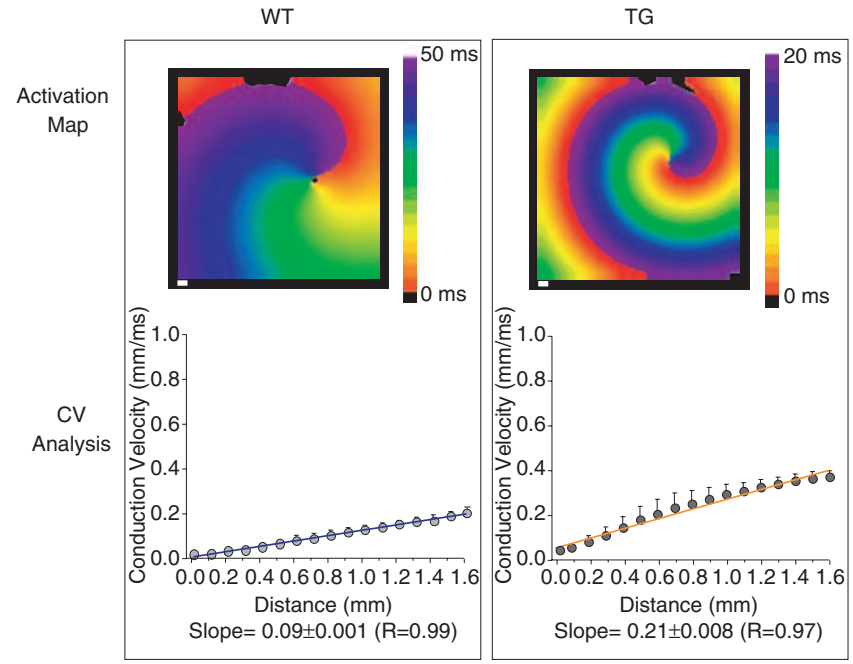

Figure 6. Conduction velocity as a function of distance from the core during reentry in computer simulations of WT (left) and TG (right) hearts
Top, activation maps. Colour scale: WT, 0–50 ms; TG, 0–20 ms. White scale bars, 1 mm. Bottom, plots of average (± S.D.) local velocity *versus* distance from the core. The blue and orange lines are weighted best-fit lines. The weighted slope (±95% confidence limit) for the WT and TG hearts are 0.09 ± 0.001 ($R = 0.99$) and 0.21 ± 0.008 ($R = 0.97$), respectively. See Supplemental material for 'WT2b2sim' and 'TG2b2sim' movies.

plotted against distance from the core. The direction of propagation was normal to the rotating wavefront. The best-fit line, weighted by the S.D. of the averaged CV was computed, and the 95% confidence limits calculated. In both cases, WT and TG, the speed of propagation increased radially from the core. CV increases from core to periphery; however, the rate of increase is appreciably higher in the simulated TG (0.21 ± 0.008 ms^{-1}, $R = 0.97$) than WT (0.09 ± 0.001 ms^{-1}, $R = 0.99$) heart. As shown by the weighted slopes ($\pm$ 95% confidence limit), there is no overlap between them, and they do not reach zero, suggesting that these slopes are different from each other and from zero.

As illustrated in Fig. 7, the experimental results are qualitatively similar to the numerical predictions. CV increased much more steeply from the core to the periphery in the TG (0.21 ± 0.03 ms^{-1}, $R = 0.9$) than the WT (0.15 ± 0.01 ms^{-1}, $R = 0.89$) heart. Moreover, the range of the weighted slopes at the 95% confidence limit is 0.14–0.16 for WT and 0.18–0.24 for TG heart. The 95% confidence range of the slopes in the WT and TG hearts indicate that they are different from each other and from zero. The same analysis performed on two other rotors from two WT hearts and two additional rotors from two TG hearts yielded the following slopes: WT, 0.13 ± 0.01 ms^{-1}, $R = 0.97$ and 0.14 ± 0.02 ms^{-1}, $R = 0.84$; TG, 0.22 ± 0.02 ms^{-1}, $R = 0.95$ and 0.27 ± 0.04 ms^{-1}, $R = 0.9$. Taken altogether, the ranges of the 95% confidence limit of the slopes from the three WT hearts overlap with each other but not with the ranges of the 95% confidence limit of the slopes from the three TG hearts. Thus the slopes in the two cases differ significantly from each other.

Overall, these data demonstrate that I_{K1} up-regulation imposes greater stability on the reentrant process in the TG heart by increasing excitability, and thereby local CV near the core. The larger outward current (lower membrane resistance) brought about by I_{K1} overexpression also reduces the space constant ($\lambda = \sim\sqrt{r_m/r_i}$; where r_m is the membrane resistance and r_i is the intracellular resistance). Simulations demonstrated that the space constant in TG heart is smaller than that in a WT heart ($\lambda = 0.43$ *versus* $\lambda = 0.66$; Fig. 17 in Supplemental material). The decrease in λ, due to the increased I_{K1}, results in reductions of both the diameter of the core and the spatial extension of its electrotonic influence (see Figs 15 and 16 in Supplemental material). Measurements of core diameter using the TSP of reentry in simulated and experimental rotors confirmed the idea that an increase in I_{K1} is accompanied by a reduction of the core size (Fig. 16 in Supplemental material,). The core diameter in simulations was 3.9 ± 0.3 mm for WT and 1.9 ± 0.1 mm for TG hearts ($P < 0.001$). In experiments, the mean core diameter for three rotors in three WT hearts was 1.06 ± 0.16 mm; the mean core diameter for three rotors in three TG hearts was 0.6 ± 0.15 mm ($P < 0.001$).

How unique are the effects of I_{K1} on rotor frequency?

In the mouse line that we are studying, I_{ss} is increased by 36% in the TG heart, whereas I_{to} and I_{Kslow} are unchanged

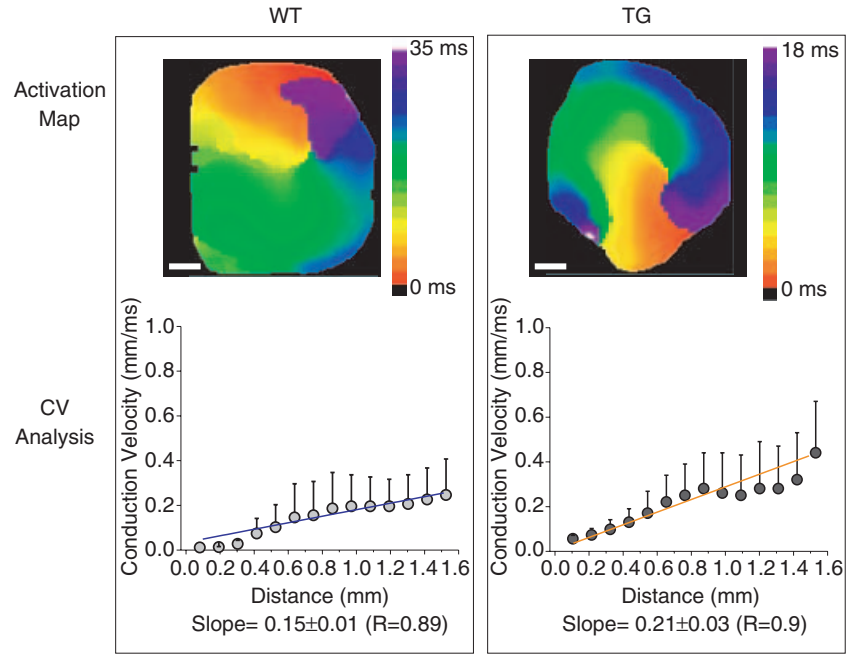

Figure 7. Experimental data of conduction velocity as a function of distance from the core during reentry in WT (left) and TG (right) hearts
Top, activation maps. Colour scale: WT, 0–35 ms; TG, 0–18 ms. White scale bars, 1 mm. Bottom, plots of average ($\pm$ S.D.) local velocity *versus* distance from the core. Blue and orange lines are weighted best-fit lines. The weighted slope ($\pm$95% confidence limit) for WT heart is 0.15 ± 0.01 ($R = 0.89$) and for TG it is 0.21 ± 0.03 ($R = 0.9$). See Supplemental material for examples of 'WTrotor' and 'TGrotor' movies.

(Li *et al*. 2004). Therefore, an important question that arises is whether enhancement of any outward current is sufficient to increase rotor frequency, similar to, or greater than that seen for I_{K1} overexpression. Figure 8*A* shows simulated APs in normal conditions and in cases where I_{ss}, I_{Kslow}, I_{to} and I_{K1} densities were each increased 2-fold. I_{to} affected the AP more in its initial repolarizing phase and I_{ss} had a small effect on the late repolarization, whereas the increase in I_{Kslow} resulted in maximal shortening of the AP. As expected, the effect of doubling I_{K1} is seen mainly during late phase 3 of the simulated AP. However, the rate of late repolarization when I_{Kslow} was increased was still slower than that seen when I_{K1} was increased. Figure 8*B* shows the rotor frequencies when increases in these currents were implemented in a 2D sheet, and rotors were induced. The rotor frequencies during increased density of I_{ss}, I_{to}, I_{Kslow} and I_{K1} were 18.5 Hz, 19.5 Hz, 20.5 Hz and 24.4 Hz, respectively, compared to 18.5 Hz in WT heart. Thus these results highlight the importance of I_{K1} by showing that, in addition to a shortened AP duration, the rate of final repolarization is a crucial determinant of rotor frequency.

Discussion

Major results

This study provides the first direct demonstration that cardiac-specific up-regulation of I_{K1} in the ventricles of a TG heart helps to control the dynamics of reentry and VF. I_{K1} contributes to AP termination (Lopatin & Nichols, 2001; Miake *et al*. 2003), and thus its up-regulation in the TG heart accelerates the final phase of AP repolarization (Zaritsky *et al*. 2001; Warren *et al*. 2003; Miake *et al*. 2003; McLerie & Lopatin, 2003; Li *et al*. 2004). During reentry, this translates into a shorter wavelength and relative membrane hyperpolarization, both of which contribute to greater Na^+ channel availability during the excitable gap and thus to increased excitability ahead of the rotating wavefront. In addition, I_{K1} overexpression augments the voltage gradient established between resting cells in the core and the active cells in its immediate surroundings. This enhances the electrotonic currents that flow continuously between resting and active cells, which further contributes not only to hasten the repolarization of the active cells but also to reduce propagation velocity very near the core (Beaumont *et al*. 1998). The end result is a steeper rise in the local CV as a function of the distance from the core and a faster, more stable rotor in TG hearts, compared to the WT hearts. Further, during reentry in the TG hearts, the non-excited cells at the very centre of the core provide a larger than normal outward conductance which decreases the likelihood of cells being excited by the depolarizing influence of their immediate, actively depolarized neighbours (sink-to-source mismatch). Consequently, the core is less likely to be invaded by the activation front, which acts to prevent tip meandering and thus to stabilize the rotor.

As discussed in a previous study in which more aggressive protocols were used (Vaidya *et al*. 1999), the ability to induce reentry in the mouse heart is usually variable and dependent on many factors, including the electrode position, stimulus strength and pacing frequency. In the present experiments, reentry in TG hearts was faster and more stable than in WT hearts. In hindsight, this is not surprising because the short APD could act to minimize wave front–wave tail interactions. In the WT mice, wave front–wave tail interaction is a plausible mechanism explaining the short life of reentrant episodes as demonstrated by the computer simulations (Fig. 14 in Supplemental material and the supporting movie of reentry in a WT 1 cm × 1 cm sheet) ('WT1b1sim'). In all likelihood, such interactions interfered with the stability of the core and led to the termination of reentry (Beaumont *et al*. 1998; Samie *et al*. 2001). On the other hand, up-regulation of I_{K1} endowed the hearts with the ability to sustain faster and longer-lasting reentry.

The mechanism of increased DF and stability in TG hearts

Our computer simulations support the idea that the mechanism by which I_{K1} controls reentry dynamics is related to its role in contributing to the rate of final phase of repolarization. Thus, although in the mouse heart, I_{K1} is one order of magnitude smaller than I_{to} and I_{Kslow}, even a 2-fold increase in the conductance of the latter two

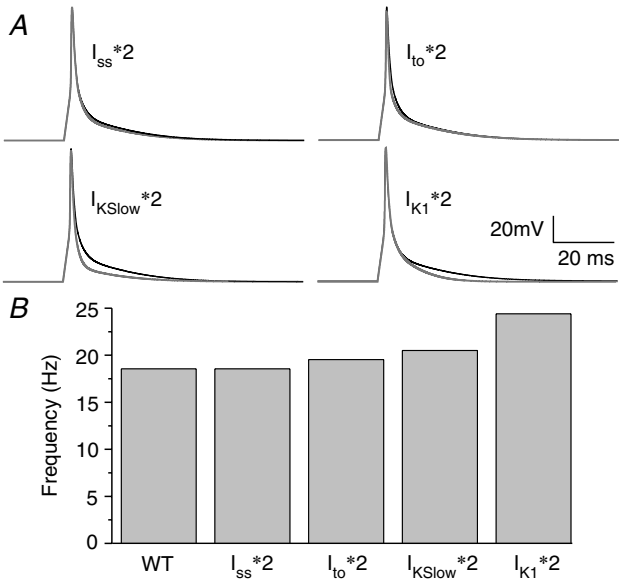

Figure 8. Simulation data showing the effects of increasing I_{ss}, I_{Kslow}, I_{to} and I_{K1} on action potential characteristics (*A*) and rotor frequencies (*B*). *2, increase 2-fold.

currents had less effect on frequency of reentry, compared to a 2-fold increase in I_{K1}. In theory, any increase in net outward current may act to increase frequency and stability of reentry in the heart. However, our data predict that, in the mouse heart, increasing the inwardly rectifying current should have a greater effect than increasing any of the other potassium currents. Indeed, as discussed above, the role of I_{K1} in controlling the resting membrane potential, the approach to threshold and the final phase of repolarization make it an important regulator of both rotor frequency and stability.

Overexpressing I_{K1} improves the excitability of the tissue during reentry. This is evident by the increased CV, as a function of distance from the core during reentry, in both numerical and biological experiments (Figs 6 and 7) secondary to membrane hyperpolarization (see Fig. 5). During reentry, I_{K1} overexpression is expected to increase the electrotonic influence of the core on its immediate surroundings (Beaumont *et al*. 1998; Samie *et al*. 2000). This influence reduces APD, and thus diminishes wavelength and increases the excitable gap near the core. In fact, analysis of the simulation data revealed that I_{K1} increase acted to minimize wavefront–wavetail interactions. In addition, the TG heart displays greater I_{Na} recovery than WT during the excitable gap because of a relative hyperpolarization and shorter wavelength, as was shown previously for simulations of chronic atrial fibrillation (Pandit *et al*. 2005). In the case of ventricular reentry in the WT heart, the relatively depolarized tissue ahead of the wavefront imposes a larger proportion of less than adequately recovered Na^+ channels, which results in lower rotor frequency and stability than for TG hearts. When the simulations were conducted using 2D sheets of 1 cm × 1 cm, the rotor from the TG heart rotated stably at 45 Hz while the WT heart underwent only approximately two rotations followed by immediate termination. These results support our hypothesis that the magnitude of the outward component of I_{K1} plays an important role in controlling the frequency of VT/VF and in determining the ability of the ventricles of the mouse to undergo stable reentry.

Core influence *versus* increased excitability

The simulations show that while CV during reentry increases throughout the 2D sheet as a result of shorter wavelength membrane hyperpolarization, and resultant Na^+ channel recovery, the magnitude of the electrotonic influence exerted by the core on its immediate surroundings also increases. The latter would be expected to reduce CV near the core. However, analysis of the local CVs during reentry in both simulations and experiments showed that not only is CV greater overall but also the slope relating CV to core distance is higher in TG than WT hearts, indicating that the excitability of the tissue is enhanced by the increased I_{K1}. This seemingly counterintuitive result finds its explanation in the reduced space constant that is a direct consequence of the increased outward current associated with I_{K1} overexpression. Thus, on the one hand, the electrotonic gradient between the unexcited core and its immediate surroundings is greater and, on the other, the rate of decay of that gradient with distance is much faster. In addition, as shown in the Supplemental material, the diameter of the core of the faster rotor in the TG heart is appreciably smaller than that of the WT heart, which necessarily reduces the spatial extension of its influence on the reentrant activity of the surrounding tissues.

Ventricular remodelling plays no role

The TG hearts used in these experiments had an increased I_{K1} density due to cardiac-specific expression of Kir2.1–GFP fusion protein under the control of the α-myosin heavy chain promoter (Li *et al*. 2004). Additional confirmation of the expression of the Kir2.1–GFP transgene in the mouse hearts that were used here is provided by probing membrane fractions of two WT and two TG hearts with Kir2.1 antibody (Fig. 1 in Supplemental material). The Western blot showed a band in both 'WT and TG lanes' at around 47 kDa, corresponding to the size of the native Kir2.1 protein. In the TG lane, a prominent band at around 70 kDa is apparent, indicating the expression of the Kir2.1–GFP transgene. It was previously reported that the line of transgenic mice we have used exhibited a trend towards cardiac hypertrophy (Li *et al*. 2004). However, our results showed that there was no significant difference in the weight of TG with respect to WT hearts (Fig. 4). In addition, probing the mRNA extracted from the LV for molecular markers of hypertrophy, showed no evidence of remodelling in TG hearts. Furthermore, detailed examination of possible compensation in ionic conductances of K^+ and Ca^{2+} channels showed that I_{K1} was the only current that was radically changed (by 1200%), whereas I_{ss} was changed only by 36% (Li *et al*. 2004). Additionally, patch-clamp experiments did not show statistically significant changes in mean membrane capacitance of isolated WT and TG myocytes (Li *et al*. 2004). Therefore, it is unlikely that the effects we have observed are caused by hypertrophic or other known ionic current compensatory changes, although subtle effects cannot be excluded.

Clinical implications

Very recently, Priori *et al*. (2005) characterized a novel form of short QT syndrome named SQTS3. Two members of a family presented with a *de novo* gain-of-function mutation in the *KCNJ2* gene that encodes for Kir2.1 channels. The ECG pattern in the two affected family members was

clearly different from those previously reported in patients affected by SQTS (Priori *et al*. 2005). In addition, screening of the *KCNJ2* gene disclosed the presence of a single base pair mutation resulting in a D172N substitution located in the second transmembrane region of the channel. Expression studies showed that the D172N mutation caused an increase in the outward component (reduced inward rectification) of the current–voltage relation of I_{K1} (Stanfield *et al*. 1994; Priori *et al*. 2005). In the study of Priori *et al*. (2005), computer simulations predicted that such an increase in outward current should accelerate terminal ventricular repolarization, as seen in the present study. Clinical electrophysiological testing of one of the mutation carriers demonstrated VF inducibility using standard premature stimulation protocols (Priori *et al*. 2005). Thus, the identification of SQTS3 has highlighted the concept that genetic abnormalities leading to gain-of-function mutations in Kir2.1 proteins may predispose to the development of tachyarrhythmias and sudden cardiac death. Although it must be noted that reduced inward rectification may have effects different from those resulting from channel overexpression, the studies presented here in transgenic mice provide novel and useful insights into the molecular mechanisms of arrhythmias in SQTS3 patients, and possibly also in other groups of patients affected by unexplained idiopathic VF.

Potential limitations

The mouse is important for modelling human disease. However, it is clear that significant differences exist in the ion channel correlates and mechanisms of the murine cardiac AP and the AP of other mammals, particularly humans. Therefore a direct extrapolation of results obtained from rodent models to humans cannot be made, and neither is it attempted here. However, it has been pointed out in many reviews and editorials (Rosen, 2000; Nerbonne, 2004) that rodent models are very relevant to the elucidation/establishment of general principles underlying cardiac arrhythmias. In this case, studying the electrophysiological phenotype of a transgenic mouse overexpressing Kir2.1 in the heart provided useful insights into the role that I_{K1} plays in the maintenance of reentry and fibrillation.

We have created a simplified Hodgkin-Huxley-type mathematical model of the mouse cardiac AP at 37°C, with fixed intra- and extracellular ionic concentrations. This clearly does not take into account the complex intracellular Ca^{2+} dynamics, as well accumulation of extracellular K^+ ions in clefts/T-tubules. Thus the potential role of currents such as the Na^+–Ca^{2+} exchanger in reentry cannot be ruled out, but a large role is unlikely in this study, given the ∼12-fold increase reported in I_{K1}, which will mask any contribution from the exchanger. Furthermore, whether Ca^{2+} release takes place and to what extent at the high frequencies (20–50 Hz) seen in this study will need further investigation. The Hodgkin-Huxley-type representation of ionic currents is less accurate than corresponding Markovian formulations. Finally, our 2D simulations do not consider anisotropy or tissue heterogeneity in APD and excitability. Despite these limitations, our simulations provide useful mechanistic insights into the plausible mechanisms underlying rotor acceleration/stability due to increased I_{K1}.

References

Bagwe S, Berenfeld O, Vaidya D, Morley GE & Jalife J (2005). Altered right atrial excitation and propagation in connexin40 knockout mice. *Circulation* **112**, 2245–2253.

Beaumont J, Davidenko N, Davidenko JM & Jalife J (1998). Spiral waves in two-dimensional models of ventricular muscle: formation of a stationary core. *Biophys J* **75**, 1–14.

Berenfeld O, Zaitsev AV, Mironov SF, Pertsov AM & Jalife J (2002). Frequency-dependent breakdown of wave propagation into fibrillatory conduction across the pectinate muscle network in the isolated sheep right atrium. *Circ Res* **90**, 1173–1180.

Bondarenko VE, Szigeti GP, Bett GC, Kim SJ & Rasmusson RL (2004). Computer model of action potential of mouse ventricular myocytes. *Am J Physiol Heart Circ Physiol* **287**, H1378–H1403.

Chomczynski P & Sacchi N (1987). Single-step method of RNA isolation by acid guanidinium thiocyanate-phenol-chloroform extraction. *Anal Biochem* **162**, 156–159.

DiFrancesco D, Ferroni A & Visentin S (1984). Barium-induced blockade of the inward rectifier in calf Purkinje fibres. *Pflugers Arch* **402**, 446–453.

Fox JJ, McHarg JL & Gilmour RF Jr (2002). Ionic mechanism of electrical alternans. *Am J Physiol Heart Circ Physiol* **282**, H516–H530.

Kubo Y, Baldwin TJ, Jan YN & Jan LY (1993). Primary structure and functional expression of a mouse inward rectifier potassium channel. *Nature* **362**, 127–133.

Li J, McLerie M & Lopatin AN (2004). Transgenic up-regulation of IK1 in the mouse heart leads to multiple abnormalities of cardiac excitability. *Am J Physiol Heart Circ Physiol* **287**, H2790–H2802.

Lopatin AN & Nichols CG (2001). Inward rectifiers in the heart: an update on I_{K1}. *J Mol Cell Cardiol* **33**, 625–638.

McLerie M & Lopatin A (2003). Dominant-negative suppression of I_{K1} in the mouse heart leads to altered cardiac excitability. *J Mol Cell Cardiol* **35**, 367–378.

Miake J, Marban E & Nuss HB (2003). Functional role of inward rectifier current in heart probed by Kir2.1 overexpression and dominant-negative suppression. *J Clin Invest* **111**, 1529–1536.

Morley GE, Vaidya D, Samie FH, Lo C, Delmar M & Jalife J (1999). Characterization of conduction in the ventricles of normal and heterozygous Cx43 knockout mice using optical mapping. *J Cardiovasc Electrophysiol* **10**, 1361–1375.

Nerbonne JM (2004). Studying cardiac arrhythmias in the mouse – a reasonable model for probing mechanisms? *Trends Cardiovasc Med* **14**, 83–93.

Pandit SV, Berenfeld O, Anumonwo JM, Zaritski RM, Kneller J, Nattel S & Jalife J (2005). Ionic determinants of functional reentry in a 2-D model of human atrial cells during simulated chronic atrial fibrillation. *Biophys J* **88**, 3806–3821.

Pandit SV, Clark RB, Giles WR & Demir SS (2001). A mathematical model of action potential heterogeneity in adult rat left ventricular myocytes. *Biophys J* **81**, 3029–3051.

Piechaczyk M, Blanchard JM, Marty L, Dani C, Panabieres F, El Sabouty S, Fort P & Jeanteur P (1984). Post-transcriptional regulation of glyceraldehyde-3-phosphate-dehydrogenase gene expression in rat tissues. *Nucleic Acids Res* **12**, 6951–6963.

Priori SG, Pandit SV, Rivolta I, Berenfeld O, Ronchetti E, Dhamoon A *et al*. (2005). A novel form of short QT syndrome (SQT3) is caused by a mutation in the KCNJ2 gene. *Circ Res* **96**, 800–807.

Rosen MR (2000). The real thing. *Circ Res* **87**, 6–7.

Samie FH, Berenfeld O, Anumonwo J, Mironov SF, Udassi S, Beaumont J, Taffet S, Pertsov AM & Jalife J (2001). Rectification of the background potassium current: a determinant of rotor dynamics in ventricular fibrillation. *Circ Res* **89**, 1216–1223.

Samie FH, Mandapati R, Gray RA, Watanabe Y, Zuur C, Beaumont J & Jalife J (2000). A mechanism of transition from ventricular fibrillation to tachycardia: effect of calcium channel blockade on the dynamics of rotating waves. *Circ Res* **86**, 684–691.

Seidman CE, Duby AD, Choi E, Graham RM, Haber E, Homcy C, Smith JA & Seidman JG (1984). The structure of rat preproatrial natriuretic factor as defined by a complementary DNA clone. *Science* **225**, 324–326.

Stanfield PR, Davies NW, Shelton PA, Sutcliffe MJ, Khan IA, Brammar WJ & Conley EC (1994). A single aspartate residue is involved in both intrinsic gating and blockage by Mg^{2+} of the inward rectifier, IRK1. *J Physiol* **478**, 1–6.

Tamaddon HS, Vaidya D, Simon AM, Paul DL, Jalife J & Morley GE (2000). High-resolution optical mapping of the right bundle branch in connexin40 knockout mice reveals slow conduction in the specialized conduction system. *Circ Res* **87**, 929–936.

Vaidya D, Morley GE, Samie FH & Jalife J (1999). Reentry and fibrillation in the mouse heart. A challenge to the critical mass hypothesis. *Circ Res* **85**, 174–181.

Warren M, Guha PK, Berenfeld O, Zaitsev A, Anumonwo JM, Dhamoon AS, Bagwe S, Taffet SM & Jalife J (2003). Blockade of the inward rectifying potassium current terminates ventricular fibrillation in the guinea pig heart. *J Cardiovasc Electrophysiol* **14**, 621–631.

Zaritsky JJ, Redell JB, Tempel BL & Schwarz TL (2001). The consequences of disrupting cardiac inwardly rectifying K^+ current (I_{K1}) as revealed by the targeted deletion of the murine Kir2.1 and Kir2.2 genes. *J Physiol* **533**, 697–710.

Zhang H, Garratt CJ, Zhu J & Holden AV (2005). Role of up-regulation of IK1 in action potential shortening associated with atrial fibrillation in humans. *Cardiovasc Res* **66**, 493–502.

Acknowledgements

This work was supported by National Heart, Lung and Blood Institute (NHLBI) grants PO1 HL039707, RO1 HL070074 and RO1 HL060843 to J.J., RO1 HL69052 to A.N.L., an American Heart Association (AHA) Scientist Development Grant to O.B. and an AHA Postdoctoral Fellowship to S.V.P.

Supplemental material

The online version of this paper can be accessed at:
DOI: 10.1113/jphysiol.2006.121475
http://jp.physoc.org/cgi/content/full/jphysiol.2006.121475/DC1
and contains supplemental material consisting of further results (with 17 figures) and seven video clips.

This material can also be found as part of the full-text HTML version available from http://www.blackwell-synergy.com